npj | computational materials

Article

Published in partnership with the Shanghai Institute of Ceramics of the Chinese Academy of Sciences

https://doi.org/10.1038/s41524-024-01237-2

Stoner instability-mediated large magnetoelectric effects in 2D stacking electrides

Zhigang Gui[1], Haiyan Zhu[1], Zhe Wang[1], M. Umar Farooq[1], Laurent Bellaiche[2] & Li Huang[1,3]

Strong magnetoelectric effects in single-phase two-dimensional (2D) materials are extremely rare in nature. Here by first-principles calculations, we find a strong magnetoelectric coupling in polar stacking bilayer Hf_2S that allows the reversal of net magnetic moments with the reversal of electric dipoles. Further analysis shows that such strong magnetoelectric effects benefit from the Stoner instability of surface Hf atoms triggered by polar stacking. Moreover, an unexpectedly large out-of-plane electric polarization (which is at least two times larger than that of bilayer BN) survives in the material, despite its metallicity. The large electric polarization is ascribed to the delocalized interlayer electrons which generally present in layered electride materials. It is quite interesting that large electric polarization, metallicity and magnetism coexist in one single-phase material. Our findings reveal rich physical phenomena to be explored in 2D stacking multiferroics and suggest an alternative way of searching for strong magnetoelectric materials with ultrathin thickness.

Multiferroic materials are a special class of multifunctional materials that possess broken space inversion symmetry, switchable polarization under external fields and magnetism. They have been reported to display varieties of intriguing physical phenomena including, but not limited to, large piezoelectric coefficients, dielectric tunability, complex structural transitions, nontrivial dipole and spin textures and magnetoelectric coupling effects, which lead to broad applications such as actuators, sensors, field-effect transistors, tunneling junctions and emergent electronics[1–6]. For applications in miniaturized memory or logic devices, it is highly desirable to have a multiferroic material as thin as a few unit-cell thickness with sharp and clean surface, robust out-of-plane (OP) electric polarization, magnetic orderings and strong magnetoelectric coupling sustainable above room temperature (RT). In this regard, multiferroicity in 2D van der Waals (vdW) materials consisting of a single or few layers offers promising alternatives. 2D materials inspired by single-atomic-layer graphene and BN has flourished and drawn great attention in the past decade[7]. Unfortunately, only a few 2D materials have been experimentally verified to be intrinsic ferroelectrics, and 2D intrinsic ferroelectric materials with OP polarization are very scare so far. For instance, in-plane (IP) ferroelectricity is observed in monolayer SnTe[8–10], while OP polarization has been reported in few-layer $CuInP_2S_6$ nanoflakes[11], In_2Se_3 with thickness as thin as three layers[12,13], $MoTe_2$ down to the single atomic layer[14,15] and Bi monolayer[16]. There are also some other computational predictions on 2D intrinsic ferroelectrics which still await experimental confirmation[17–19]. On the other hand, 2D intrinsic multiferroic materials with strong magnetoelectric effects are even more scare. $CuCrP_2S_6$, $Ti_3C_2T_x$ MXene and NiI_2 have only been recently confirmed to show both ferroelectricity and magnetism[20–22]. In addition, some approaches have been proposed to induce multiferroicity in 2D materials[23–31]. Among these, polar stacking of 2D vdW materials is a straightforward and efficient way[32–34]. However, stacking-based 2D multiferroics typically display a notably small polarization and minimal intrinsic coupling between ferroelectricity and magnetism due to their inherent separation in origins[32–39]. Then the question remains: is it possible to achieve a large electric polarization (compared to known stacking 2D ferroelectrics) and strong magnetoelectric coupling simultaneously in a single-phase vdW material under polar stacking?

In this work, using first-principles calculations, we show that bilayer Hf_2S presents a much larger OP electric polarization by interlayer stacking despite of its metallicity, as compared to most stacking 2D ferroelectrics. This large electric dipole is revealed to stem from the delocalized interlayer electrons. In addition, there is an unexpected emergence of net magnetization which can be ascribed to Hf atoms at the surface layers, given the fact that the bulk phase is nonmagnetic while the monolayer phase is antiferromagnetic. More importantly, a strong magnetoelectric coupling is

[1]Department of Physics & Academy for Advanced Interdisciplinary Studies, Southern University of Science & Technology, Shenzhen, Guangdong 518055, China. [2]Physics Department and Institute for Nanoscience and Engineering, University of Arkansas, Fayetteville, AR 72701, USA. [3]Quantum Science Center of Guangdong-Hong Kong-Macao Greater Bay Area (Guangdong), Shenzhen 518045, China. e-mail: huangl@sustech.edu.cn

identified that ensures the reversal of magnetization with the switching of electric dipoles. The coexistence of polar electric dipole, magnetization and metallicity in one 2D material makes it a rare multiferroic metal. Our work presents an alternative way of searching for multiferroics with OP polarization and strong magnetoelectric couplings in ultrathin materials.

Results and discussion

Structural and ferroelectric properties of Hf_2S bilayer

Hf_2S is a known example of layered electride materials which are characterized by the presence of electrons trapped within the vdW gap region between layers (also referred as interlayer anionic electrons)[40]. Bulk Hf_2S can be viewed as consisting of two layers of which one is rotated by 180° with respect to the other one. The upper panel of Fig. 1a gives the bulk structure (with space group $P6_3/mmc$). For each monolayer, each S atom is sandwiched by the top and bottom Hf layers and bonds to six Hf atoms. Neither the bulk nor the bilayer with the same stacking order as in the bulk give a net electric dipole, due to the presence of spatial inversion symmetry. However, with the polar stacking shown in Fig.1b, bilayer Hf_2S permits a net electric dipole. In this polar stacking, the nominal anion S atoms from the lower layer are situated right below the cations Hf from the upper layer, while the cations Hf from the lower layer are located right below the hollow centers from the upper layer (see the top view in Fig.1b). Such polar stacking gives a large electric dipole (0.014 eÅ/u.c.) pointing downwards, which is much larger than that (0.003 eÅ/u.c.) of the polar stacking bilayer BN[37]. Phonon dispersion in Supplementary Fig. 1 indicates its dynamical stability.

To understand how the electric dipole forms, the charge redistribution is shown in Fig. 1c under such polar stacking, by plotting the differential charge density between the bilayer and two monolayers (see caption for details). Charge accumulation (shown in yellow color) occurs at X_2 along the Hf-S vertical segment (denoted by dashed line) and around the interlayer anionic center X_{1u}, while charge depletion occurs around the interlayer anionic center X_{1d}. Notably, the charges transferred from around X_{1d} to X_2 lead to the generation of a downward electric dipole and the disappearance of the interlayer anionic electron at X_{1d} (see Supplementary Fig. 2 for comparison). In the case of the polar stacking of other 2D bilayer materials reported in the literature such as BN, the electric dipole comes from the distorted electron cloud along the cation-anion vertical segment (the one denoted by the dashed line)[37]. Here, the large electric dipole in bilayer Hf_2S additionally benefits from the interlayer anionic electron which is delocalized and able to relocate during interlayer stacking shifting (see Supplementary Fig. 2), which may not be the case for other layered electrides with strongly localized interlayer anionic electron (e.g., see Gd_2C in Supplementary Fig. 5). To demonstrate that it can be ferroelectric, that is the electric dipole can reverse under an external electric field, an upper bound for the switching barrier is then estimated by means of the Nudged Elastic band (NEB) method[41], which is 125 meV/f.u., as shown in Fig. 1d. This implies that the electric dipole may be reversible through interlayer sliding from the perspective of the small switching barrier (see also Supplementary Table 3).

Interestingly, Fig. 2a, b provide the atom-resolved band structure and density of states for the polar stacking Hf_2S bilayer, which clearly shows that the system remains metallic. Contrary to the common belief that ferroelectricity and metallicity are mutually exclusive, we show here that bilayer Hf_2S is a potential "ferroelectric" metal with coexisting electric dipoles and conducting free carriers. By further inspecting the band structure and density of states, one can see that there are more electronic states contributed from the top and down surface regions than the regions near the vdW gap at the Fermi level, which means that a large portion of free carriers is located at surfaces. While from Fig. 1c, it has been already demonstrated that the ferroelectric dipoles mostly come from the electron redistribution near the vdW gap. The space separation of free carriers and ferroelectric dipoles may lead to weak screening, which sustains their coexistence[42].

Electronic and magnetic properties of Hf_2S bilayer

Now, let us take a closer look at the electronic properties of the polar stacking bilayer Hf_2S. As compared to the nonmagnetic and antiferromagnetic nature of the bulk and nonpolar stacking bilayer Hf_2S (see Supplementary Fig. 3), both the band structure and density of states indicate that the polar bilayer Hf_2S is a system with a net magnetization instead. As similar to the monolayer case, the local magnetic moment of Hf is thought to be of Stoner type and to result from the large 5d orbital-derived states of the surface $Hf^{1,2}$ atoms (denoted by Hf^1 on the bottom surface and Hf^2 on the top surface) around the Fermi level (see Supplementary Fig. 4), which is in-line with previous reports[43]. Due to the fact that Hf 5d orbital is quite delocalized (see Fig. 2a, b), the on-site Coulomb interactions between them and their exchange splittings are likely to be not large. As a result, no band gap opens at the Fermi level. The calculated magnetic moments of the surface Hf atom are around 0.43 μ_B and 0.08 μ_B for Hf^1 and Hf^2, respectively, with their directions remaining antiparallel. The net magnetism in this polar bilayer Hf_2S is found to be around 0.35 μ_B/f.u., which mainly comes from the inequivalence of Hf^1 and Hf^2 atoms at the two opposite surfaces. Figure 3a shows the isosurface of the magnetization density for the polar stacking

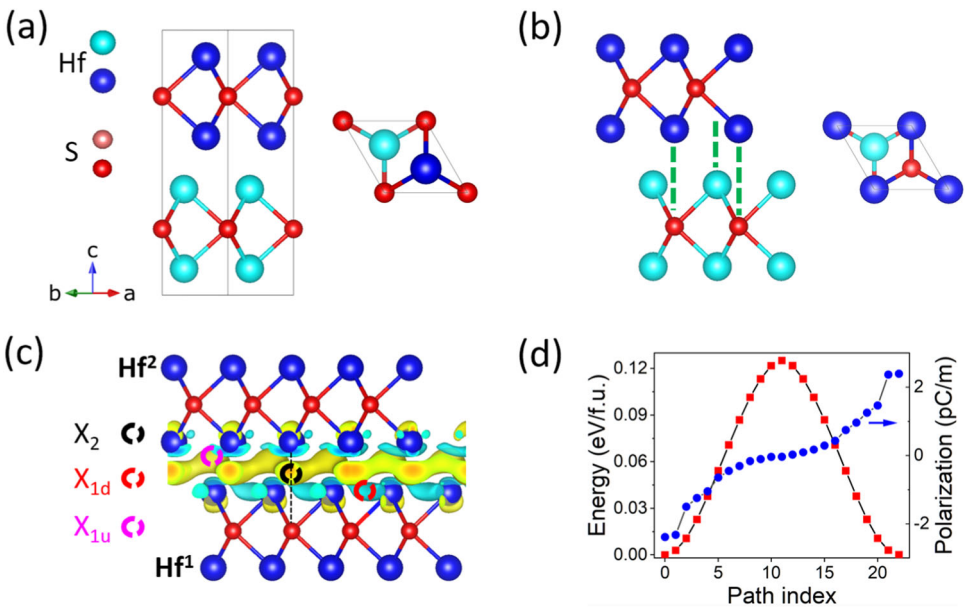

Fig. 1 | Cystal structures and ferroelectricity of bulk and the polar stacking bilayer of Hf_2S. a The crystal structure for bulk Hf_2S: side view (left) and top view (right). **b** The polar stacking of bilayer: side view (left) and top view (right). **c** Isosurface for differential charge density between the polar stacking bilayer Hf_2S and two single monolayers with the same atomic positions. The value is set to 20% of the maximum. The markers X_2, X_{1d} and X_{1u} points present the interlayer anionic electron charge centers in bilayer Hf_2S. **d** The homogeneous switching barrier (left axis) and the corresponding polarization (right axis) from NEB calculation.

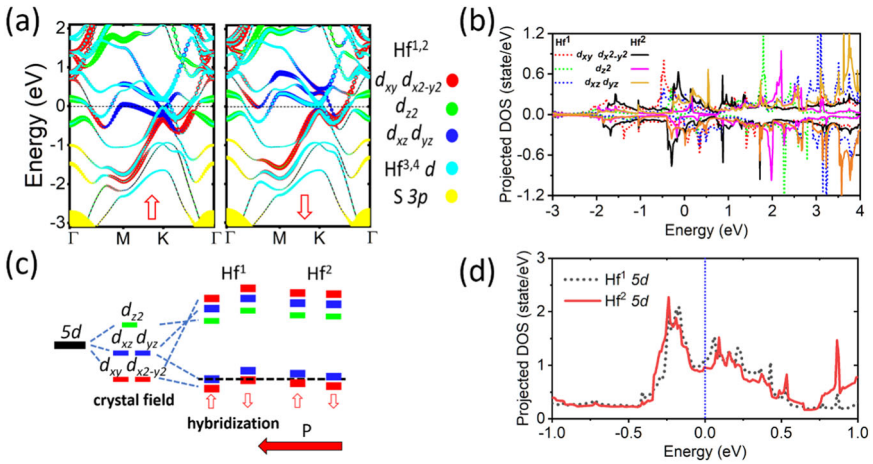

Fig. 2 | Electronic properties of polar stacking bilayer Hf_2S. a The projected spin-polarized electronic band structure. **b** The projected density of states for Hf^1 (dotted lines) and Hf^2 (solid lines). **c** Schematic of Hf^1 5*d* orbitals' splitting due to crystal field, band hybridization and exchange interaction. **d** The projected density of states of 5d orbitals from Hf^1 (black dotted line) and Hf^2 (red solid line) in nonmagnetic case.

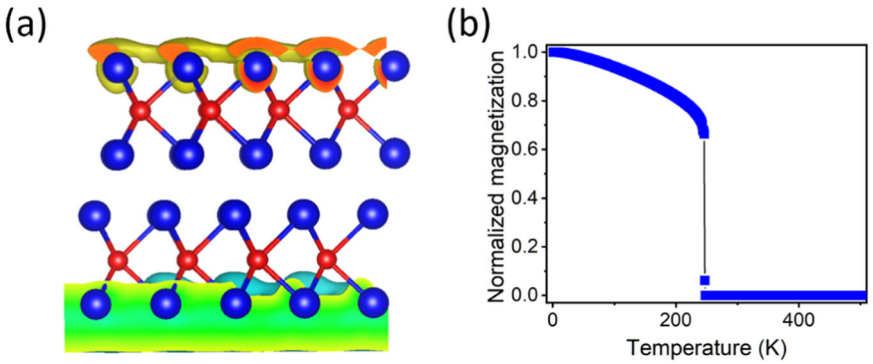

Fig. 3 | Magnetic properties of Hf_2S. a Isosurface of the magnetic charge density. The value is set to 20% of the maximum. **b** Simulated magnetization versus temperature.

bilayer. The magnetization density from up and down spin channels are noticeably inequivalent and located around Hf atoms at the two opposite surfaces, as aforementioned. To better understand the difference in magnitude between the magnetic moments of Hf on the two opposite surfaces, a detailed analysis on the decomposition of the electronic structures is warranted. The atom-resolved band structures and density of states indicate that the Hf 5d orbital-derived states are split into three subsets a_{1g} (d_z^2), e_{1g} ($d_{x^2-y^2}$, d_{xy}) and e_{2g} (d_{xz}, d_{yz}) with the trigonal crystal field, as shown in Fig. 2c. Note that the Hf 5d orbitals are not localized but rather quite dispersive. For instance, the Hf $5d_{xy}$, $5d_{xz}$-derived states extend almost all over the energy window (over 8 eV in Fig. 2a, b). Therefore, the three subsets will further hybridize and split, as shown in the schematic diagram in Fig. 2c. The occupations among these states are thus different for Hf^1 and Hf^2 atoms. Due to the electron redistribution occurring mainly in the vdW gap in the polar stacking bilayer Hf_2S, the generation of ferroelectric dipoles then leads to a potential difference between Hf^1 and Hf^2 atoms. For the dipole moment pointing downward, the energy levels derived from the orbitals (particularly d orbitals) of Hf^2 atoms will shift higher. Figure 2d gives the projected density of states from Hf^1 and Hf^2 atoms on the surfaces for the nonmagnetic case, which indicates that there is a decrease in the density of states of Hf^2 at the Fermi level, as compared to that of Hf^1 (see also Fig. S4b). As mentioned above, the magnetism of Hf atom is deemed to be of Stoner type. Such decrease of density of states suggests a weakening of the Stoner magnetism, which leads to a further decrease of the exchange splitting and occupation redistribution among Hf^2 d-derived orbitals. Figure 2b clearly shows that there is more (less) occupation of e_{1g} (e_{2g}) subset in the spin up (down) channel for Hf^2, which ultimately leads to a reduction of the spin magnetic moment of Hf^2 and a sizeable net spin magnetic moment that makes the system ferrimagnetic (see Fig. 3a). Such delicate balance between band filling and the Stoner magnetism instability under the influence of the inherent electric field from the polar stacking is proposed to underlie the strong magnetoelectric effect discussed later.

To further examine the stability of the ferrimagnetism present in the system, conventional energy mapping method is adopted to extract the exchange parameters between neighboring magnetic Hf atoms (see Supplementary Fig. 6 for more details). Considering that the magnetic moments on the $Hf^{3,4}$ (near the vdW gap) and Hf^2 ions are comparably small and negligible, magnetic interactions for as far as third nearest neighbors on the bottom surface are tested to be sufficient. With the extracted exchange parameters, a Curie temperature of around 248 K is estimated by the Monte Carlo simulations (Fig. 3b and see Supplementary Fig. 6 for details).

Magnetoelectric coupling and its mechanism

As shown above, the polar stacking which leads to 'ferroelectricity" also generates net magnetization in bilayer Hf_2S, which suggests a possible correlation between ferroelectricity and ferrimagnetism in this material, and thus makes the polar stacking Hf_2S bilayer a potential multiferroic-type material with magnetoelectric coupling. To demonstrate it, we first turn to the evolution of magnetism during the switching of ferroelectric polarization. As it has been shown in Fig. 1d, the switching through interlayer sliding is possible in the studied material. Figure 4a shows a schematic of the proposed switching process of ferroelectric dipoles and the accompanied evolution of magnetism. At stage I, the system is in one of its degenerate ground states, i.e., with electric polarization pointing downward and magnetization pointing to the right. At stage II, with the reduction of the electric polarization by sliding the top layer to the left, the magnetic moment of Hf^2 increases, while that of Hf^1 remains almost the same. Consequently, the net magnetic moment decreases. At stage III, with the increase of the magnetic

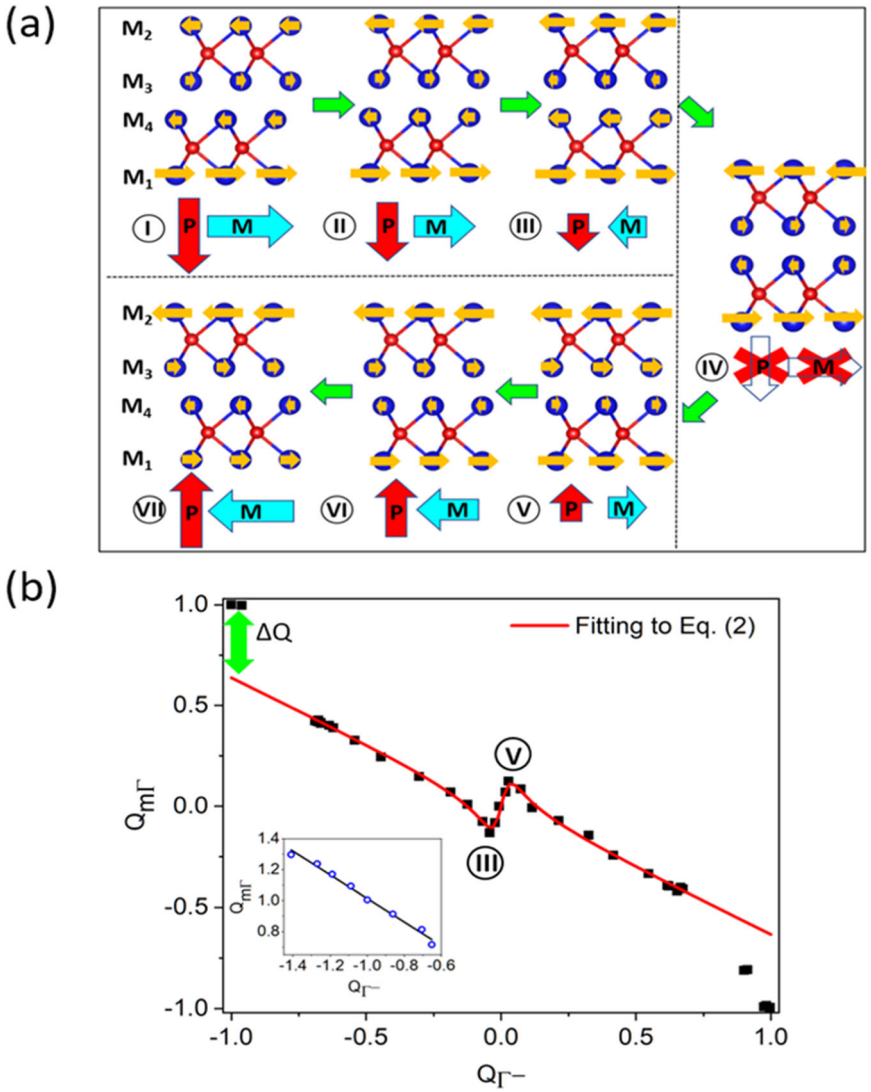

Fig. 4 | Magnetoelectric coupling. a Snapshots of electric and spin polarization in the proposed switching process. **b** Magnetization dependence on the electric polarization during the switching process. Fitting is marked by solid line. ΔQ gives the value difference of magnetic order parameter between DFT calculation and the fitting. The inset shows a good linear dependence between the magnetic and electrical order parameters.

moment of Hf^2 and Hf^4, the overall net magnetization further decreases and then changes its direction and points to left. At stage IV, the ferroelectric polarization disappears, and the magnetic moment of Hf^2 increases to be the same as that of Hf^1 in magnitude but antiparallel in direction, and therefore no net magnetization exists.

At stage V, the electric polarization reverses its direction to point upward and increases in magnitude, while the magnetic moment of Hf^4 (Hf^3) starts to decrease (increase) in magnitude due to the similar reason discussed in Fig. 2c and a net magnetization emerges and reverses its direction to the right. At stage VI, with the further decrease of the magnetic moment of Hf^1, the net magnetization changes its direction again and points to left. At stage VII, the system goes into an equivalent state in which the electric polarization and net magnetization arrive to the same values but with their directions reversed with respect to their initial states at stage I. Such direct correlation between ferroelectricity and ferrimagnetism suggests an inherent magnetoelectric coupling in the system.

To get an insight of the magnetoelectric coupling in this system, a phenomenological potential is given below based on the behaviors of two coupled order parameters shown in Figs. 4b and S7. As implied above and by Supplementary Fig. 7, it is clear that the net spin magnetization/polarization is stabilized by the electric polarization and thus considered as a secondary order parameter. To simplify the form of the potential, only two order parameters are included. One order parameter Q_{Γ^-} denotes the electric polarization and the other one Q_{mG} characterizes the net spin polarization (i.e., proportional to $M_{Hf}^1 + M_{Hf}^2 + M_{Hf}^3 + M_{Hf}^4$). Here, $Q_{\Gamma^-}(Q_{mG}) = \pm 1$ corresponds to the electric polarization (spin polarization) of the ground states and different signs mean the reversal of their direction. Neglecting high-order coupling terms and considering the fact that the electric (spin) polarization here is primary (secondary), the potential is given by

$$\begin{aligned} H_L = \; & H_0 + C_{20}Q_{\Gamma^-}^2 + C_{40}Q_{\Gamma^-}^4 + C_{02}Q_{mG}^2 \\ & + C_{11}Q_{\Gamma^-}Q_{mG} + C_{21}Q_{\Gamma^-}^2Q_{mG} + C_{31}Q_{\Gamma^-}^3Q_{mG} + C_{12}Q_{\Gamma^-}Q_{mG}^2 + C_{22}Q_{\Gamma^-}^2Q_{mG}^2 \end{aligned} \quad (1)$$

where H_0 is the potential energy of the fictitious high-symmetric phase (where Q_{Γ^-} and Q_{mG} is zero) and C's are coefficients. After minimizing the energy with respect to Q_{mG}, one can get

$$Q_{mG} = -\frac{C_{11}Q_{\Gamma^-} + C_{21}Q_{\Gamma^-}^2 + C_{31}Q_{\Gamma^-}^3}{2C_{02} + 2C_{12}Q_{\Gamma^-} + 2C_{22}Q_{\Gamma^-}^2} \quad (2)$$

For the system studied here, C_{40}, C_{02} and C_{22} are positive, while C_{31} and C_{20} are negative in accord with Figs. 1d, 4a. Generally, as it can be inferred from Eq. (2), the spin polarization (proportional to Q_{mG}) decreases in an almost linear fashion with the electric polarization (proportional to Q_{Γ^-}) when Q_{Γ^-} is large in magnitude, while it evolves as the summation of linear and cubic terms of Q_{Γ^-} when Q_{Γ^-} is small (Fig. 4b). Quantitatively, as clearly shown in Fig. 4b, Eq. (2) is in good agreement with the data points

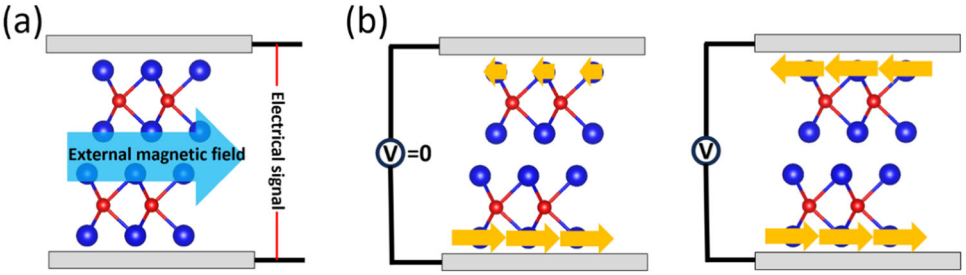

Fig. 5 | Schematics for possible potential applications. a Magnetic field sensor. **b** Magnetoelectric magnetoresistance.

(black square) by the fitting denoted by red solid line (the fitted parameters are given in Supplementary Table 2). Such behavior is rarely reported in 2D materials. The presence of such linear and cubic coupling terms in spin polarization without the inclusion of spin-orbit coupling indicates a strong magnetoelectric coupling, which is in great contrast to that found in conventional multiferroic materials such as $BiFeO_3$, $TbMnO_3$ and in known 2D multiferroics[20,22,23,32,34,44,45]. Note that the deviation from the fitting line at the end points is likely due to the instability of Stoner magnetism (see Supplementary Fig. 8), which is another manifestation of strong magnetoelectric coupling. Considering the metallic nature of the material, the minor contribution of pure carrier-mediated magnetoelectric effect cannot be ruled out[46]. Additionally, the inset of Fig. 4b shows the dependence between magnetic and electrical polarization with the ground-state crystal structure. A good linear relationship is clearly observed within the given window, which implies a giant tunability of magnetization through electric polarization or vice versa. Such properties can be practically useful for functional devices.

Proposed functional devices

In Fig. 5, schematics of two potential applications with bilayer Hf_2S are shown, taking advantage of its strong magnetoelectric effects and metallic properties. Figure 5a presents a possible magnetic field sensor. The presence of an external perturbative magnetic field can induce a change in the magnetic order that is strongly coupled to the electric polarization (see the inset of Fig. 4b). Then the change in electric polarization can be detected by charge flow. Figure 5b gives an ultrathin device based on magnetoelectric magnetoresistance. An applied electric field can efficiently tune the magnetic moments of Hf^2 on the top layer by manipulating the Stoner instability (see Fig. 2c and its discussion). Such tunability can be continuous. Considering the spin-dependent scattering within the layers[47], electrical resistivity varies with the change of the magnetic ordering, which may be further utilized in a similar way as conventional resistors.

We also note that it may be challenging to separate bulk electrides into individual layers due to the strong interlayer electrostatic interaction. Given the fact that few-layered electrides in ultrahigh vacuum have been obtained experimentally[48,49], we also consider the polar stackings of four, six and eight layers of Hf_2S, which exhibits less prominent but qualitatively similar behaviors as those in the bilayer case (see Supplementary Fig. 9 and Supplementary Table 3).

In summary, an unexpectedly large polarization contributed by the delocalized interlayer anionic electrons in bilayer Hf_2S electride is identified. Meanwhile, a coexistence of ferroelectricity and metallicity, which are supposed to be mutually exclusive in a single-phase material, is predicted for this system. Besides that, the polar stacking bilayer Hf_2S also exhibits a net spin polarization resulting from the uncompensated magnetic moments of Hf atoms located at the two opposite surfaces. Furthermore, the spin magnetization is intrinsically generated and coupled to the electric polarization through a complex dependence corroborated by a phenomenological model. The intriguing combination of electric polarization, metallicity and strong magnetoelectric effects of a novel origin in 2D materials is extremely rare in nature. Similar phenomena are also observed in other systems such as the polar stacking bilayer Hf_2Te and Zr_2S from our further calculations. Our findings therefore extend the emerging realm of 2D multiferroics and provide a new perspective for searching for strong magnetoelectric effects in ultrathin materials.

Methods

Density functional theory calculations

The calculations were performed within the density functional theory (DFT) by using the projector augmented wave (PAW) method, as implemented in the VASP code[50–53]. The revised generalized gradient approximation (GGA) with Perdew-Burke-Ernzerhof (PBE)[54] was used to treat the exchange-correlation interactions and tested to give good bulk lattice constants[43,55]. The energy cutoff for the plane-wave basis set is 400 eV (convergence tests have been shown in Supplementary Fig. 10). The *k*-point sampling was performed with a Monkhorst–Pack scheme of a $27 \times 27 \times 1$ grid with the Γ point included. The convergence criteria for the Hellmann-Feynman force and total energy were set at 0.005 eV/Å and 10^{-7} eV, respectively, for structural relaxations. The polarization is calculated by a direct integration of electronic charge density multiplied by the position vector over space within a proper slab shape. Phonon dispersion is calculated with the Phonopy package[56,57]. A vacuum space of about 18 Å was used to minimize false interactions between periodic images and nonlocal van der Waals interaction between layers is captured by the optB86b-vdW functional[58]. The correlation effects of 5d electrons in Hf were examined and found not to alter our results qualitatively, as seen from Supplementary Table 1. We thus ignore the Hubbard U correction in our calculations, as done in previous reports[43,59]. The magnetic ground state is confirmed by Monte Carlo simulation[60].

Data availability

The data supporting the findings of this study are available within this article and its Supplementary Information. Additional data that support the findings of this study are available from the corresponding author on reasonable requests.

Received: 7 October 2023; Accepted: 29 February 2024;
Published online: 12 March 2024

References

1. Scott, J. F. & Paz de Araujo Carlos, A. Ferroelectric memories. *Science* **246**, 1400–1405 (1989).
2. Ahn, C. H., Triscone, J. M. & Mannhart, J. Electric field effect in correlated oxide systems. *Nature* **424**, 1015–1018 (2003).
3. Zhuravlev, M. Y., Sabirianov, R. F., Jaswal, S. S. & Tsymbal, E. Y. Giant electroresistance in ferroelectric tunnel junctions. *Phys. Rev. Lett.* **94**, 246802 (2005).
4. Scott, J. F. Applications of modern ferroelectrics. *Science* **315**, 954–959 (2007).
5. Garcia, V. et al. Giant tunnel electroresistance for non-destructive readout of ferroelectric states. *Nature* **460**, 81–84 (2009).
6. Guo, R. et al. Non-volatile memory based on the ferroelectric photovoltaic effect. *Nat. Commun.* **4**, 1990 (2013).

7. Geim, A. K. & Novoselov, K. S. The rise of graphene. *Nat. Mater.* **6**, 183–191 (2007).
8. Chang, K. et al. Discovery of robust in-plane ferroelectricity in atomic-thick SnTe. *Science* **353**, 274–278 (2016).
9. Fei, R., Kang, W. & Yang, L. Ferroelectricity and phase transitions in monolayer Group-IV monochalcogenides. *Phys. Rev. Lett.* **117**, 097601 (2016).
10. Higashitarumizu, N. et al. Purely in-plane ferroelectricity in monolayer SnS at room temperature. *Nat. Commun.* **11**, 2428 (2020).
11. Liu, F. et al. Room-temperature ferroelectricity in $CuInP_2S_6$ ultrathin flakes. *Nat. Commun.* **7**, 12357 (2016).
12. Ding, W. et al. Prediction of intrinsic two-dimensional ferroelectrics in In_2Se_3 and other III_2-VI_3 van der Waals materials. *Nat. Commun.* **8**, 14956 (2017).
13. Zhou, Y. et al. Out-of-plane piezoelectricity and ferroelectricity in layered α-In_2Se_3 nanoflakes. *Nano Lett.* **17**, 5508–5513 (2017).
14. Shirodkar, S. N. & Waghmare, U. V. Emergence of ferroelectricity at a metal-semiconductor transition in a 1T monolayer of MoS_2. *Phys. Rev. Lett.* **112**, 157601 (2014).
15. Yuan, S. et al. Room-temperature ferroelectricity in MoTe2 down to the atomic monolayer limit. *Nat. Commun.* **10**, 1775 (2019).
16. Gou, J. et al. Two-dimensional ferroelectricity in a single-element bismuth monolayer. *Nature* **617**, 67–72 (2023).
17. Qi, L., Ruan, S. & Zeng, Y.-J. Review on recent developments in 2D ferroelectrics: theories and applications. *Adv. Mater.* **33**, 2005098 (2021).
18. Lin, L.-F., Zhang, Y., Moreo, A., Dagotto, E. & Dong, S. Frustrated dipole order induces noncollinear proper ferrielectricity in two dimensions. *Phys. Rev. Lett.* **123**, 067601 (2019).
19. Kruse, M. et al. Two-dimensional ferroelectrics from high throughput computational screening. *npj Comput. Mater.* **9**, 45 (2023).
20. Wang, X. et al. Electrical and magnetic anisotropies in van der Waals multiferroic $CuCrP_2S_6$. *Nat. Commun.* **14**, 840 (2023).
21. Tahir, R. et al. Multiferroic and ferroelectric phases revealed in 2D $Ti_3C_2T_x$ MXene film for high performance resistive data storage devices. *npj 2D Mater. Appl.* **7**, 7 (2023).
22. Lai, Y. et al. Two-dimensional ferromagnetism and driven ferroelectricity in van der Waals $CuCrP_2S_6$. *Nanoscale* **11**, 5163–5170 (2019).
23. Zhang, J.-J. et al. Type-II multiferroic $Hf_2VC_2F_2$ MXene monolayer with high transition temperature. *J. Am. Chem. Soc.* **140**, 9768–9773 (2018).
24. Chen, S. et al. Unconventional distortion induced two-dimensional multiferroicity in a CrO_3 monolayer. *Nanoscale* **13**, 13048–13056 (2021).
25. Ai, H. et al. Ferroelectricity coexisted with p-orbital ferromagnetism and metallicity in two-dimensional metal oxynitrides. *npj Comput. Mater.* **8**, 60 (2022).
26. Li, Y., Yang, B., Xu, S., Huang, B. & Duan, W. Emergent phenomena in magnetic two-dimensional materials and van der Waals Heterostructures. *ACS Appl. Electron. Mater.* **4**, 3278–3302 (2022).
27. Sun, H. et al. Prediction of tunable room-temperature ferromagnetism, ferroelectricity, and ferroelasticity in a CrNCl monolayer. *Appl. Phys. Lett.* **123**, 042901 (2023).
28. Tang, C. & Du, A. Perspective on computational design of two-dimensional materials with robust multiferroic coupling. *Appl. Phys. Lett.* **122**, 130502 (2023).
29. Tang, C., Zhang, L., Sanvito, S. & Du, A. Enabling room-temperature triferroic coupling in dual transition-metal dichalcogenide monolayers via electronic asymmetry. *J. Am. Chem. Soc.* **145**, 2485–2491 (2023).
30. Wang, C., You, L., Cobden, D. & Wang, J. Towards two-dimensional van der Waals ferroelectrics. *Nat. Mater.* **22**, 542–552 (2023).
31. Yu, G., Pan, A. & Chen, M. Interface engineering of ferroelectricity in thin films of thiophosphate ABP_2X_6 (A = Cu, Ag; B = In, Bi, Cr, V; X = S, Se). *Phys. Rev. B* **104**, 224102 (2021).
32. Liu, X., Pyatakov, A. P. & Ren, W. Magnetoelectric coupling in multiferroic bilayer VS2. *Phys. Rev. Lett.* **125**, 247601 (2020).
33. Sun, W. et al. $LaBr_2$ bilayer multiferroic moiré superlattice with robust magnetoelectric coupling and magnetic bimerons. *npj Comput. Mater.* **8**, 159 (2022).
34. Wu, Y. et al. Coexisting ferroelectric and ferrovalley polarizations in bilayer stacked magnetic semiconductors. *Nano Lett.* **23**, 6226–6232 (2023).
35. Yang, B. et al. Realization of semiconducting layered multiferroic heterojunctions via asymmetrical magnetoelectric coupling. *Phys. Rev. B* **103**, L201405 (2021).
36. Gong, C., Kim, E. M., Wang, Y., Lee, G. & Zhang, X. Multiferroicity in atomic van der Waals heterostructures. *Nat. Commun.* **10**, 2657 (2019).
37. Wang, Z., Gui, Z. & Huang, L. Sliding ferroelectricity in bilayer honeycomb structures: a first-principles study. *Phys. Rev. B* **107**, 035426 (2023).
38. Li, L. & Wu, M. Binary compound bilayer and multilayer with vertical polarizations: two-dimensional ferroelectrics, multiferroics, and nanogenerators. *ACS Nano* **11**, 6382–6388 (2017).
39. Vizner Stern, M. et al. Interfacial ferroelectricity by van der Waals sliding. *Science* **372**, 1462–1466 (2021).
40. Inoshita, T., Jeong, S., Hamada, N. & Hosono, H. Exploration for two-dimensional electrides via database screening and Ab initio calculation. *Phys. Rev. X* **4**, 031023 (2014).
41. Mills, G., Jónsson, H. & Schenter, G. K. Reversible work transition state theory: application to dissociative adsorption of hydrogen. *Surf. Sci.* **324**, 305–337 (1995).
42. Gui, Z. et al. Improper multiferroiclike transition in a metal. *Phys. Rev. B* **105**, L180101 (2022).
43. Liu, S., Wang, C., Jeon, H., Jia, Y. & Cho, J.-H. Emerging two-dimensional magnetism in nonmagnetic electrides Hf_2X (X = S, Se, Te). *Phys. Rev. B* **105**, L220401 (2022).
44. Chu, Y.-H. et al. Electric-field control of local ferromagnetism using a magnetoelectric multiferroic. *Nat. Mater.* **7**, 478–482 (2008).
45. Kimura, T. et al. Magnetic control of ferroelectric polarization. *Nature* **426**, 55–58 (2003).
46. Rondinelli, J. M., Stengel, M. & Spaldin, N. A. Carrier-mediated magnetoelectricity in complex oxide heterostructures. *Nat. Nanotechnol.* **3**, 46–50 (2008).
47. Baibich, M. N. et al. Giant magnetoresistance of (001)Fe/(001)Cr magnetic superlattices. *Phys. Rev. Lett.* **61**, 2472–2475 (1988).
48. Druffel, D. L. et al. Experimental demonstration of an electride as a 2D material. *J. Am. Chem. Soc.* **138**, 16089–16094 (2016).
49. Oh, Y. et al. Electric field effect on the electronic structure of 2D Y2C electride. *2D Mater.* **5**, 035005 (2018).
50. Hohenberg, P. & Kohn, W. Inhomogeneous electron gas. *Phys. Rev.* **136**, B864–B871 (1964).
51. Kohn, W. & Sham, L. J. Self-consistent equations including exchange and correlation effects. *Phys. Rev.* **140**, A1133–A1138 (1965).
52. Blöchl, P. E. Projector augmented-wave method. *Phys. Rev. B* **50**, 17953–17979 (1994).
53. Kresse, G. & Furthmüller, J. Efficient iterative schemes for ab initio total-energy calculations using a plane-wave basis set. *Phys. Rev. B* **54**, 11169–11186 (1996).
54. Perdew, J. P., Burke, K. & Ernzerhof, M. Generalized gradient approximation made simple. *Phys. Rev. Lett.* **77**, 3865–3868 (1996).
55. Kang, S. H. et al. Water- and acid-stable self-passivated dihafnium sulfide electride and its persistent electrocatalytic reaction. *Sci. Adv.* **6**, eaba7416 (2020).
56. Togo, A., Chaput, L., Tadano, T. & Tanaka, I. Implementation strategies in phonopy and phono3py. *J. Phys. Condens. Matter* **35**, 353001 (2023).
57. Togo, A. & Tanaka, I. First principles phonon calculations in materials science. *Scr. Mater.* **108**, 1–5 (2015).
58. Klimeš, J., Bowler, D. R. & Michaelides, A. Van der Waals density functionals applied to solids. *Phys. Rev. B* **83**, 195131 (2011).

59. Zhang, J.-F. et al. Magnetic surface on nonmagnetic bulk of electride Hf2S. *J. Phys. Chem. C.* **127**, 696–701 (2023).
60. Evans, R. F. L. et al. Atomistic spin model simulations of magnetic nanomaterials. *J. Phys.Condens. Matter* **26**, 103202 (2014).

Acknowledgements

This work was supported by the Ministry of Science and Technology of the People's Republic of China (no. 2022YFA1402903) and the National Natural Science Foundation of China under Grant No. 12004160 and 12374059. Z.G. also acknowledges the financial support from Shenzhen Science and Technology Program (Grant No. KQTD20190929173815000), and Guangdong Innovative and Entrepreneurial Research Team Program (Grant No. 2019ZT08C044). Part of this work was supported by the Quantum Science Center of Guangdong-Hong Kong-Macao Greater Bay Area (Guangdong) and the Open Project of Guangdong Provincial Key Laboratory of Magnetoelectric Physics and Devices, No. 2022B1212010008. L.B. acknowledges support from the Vannevar Bush Faculty Fellowship (VBFF, Grant No. N00014-20-1-2834) from the Department of Defense. Computational time was supported by the Center for Computational Science and Engineering of Southern University of Science and Technology and the Major Science and Technology Infrastructure Project of Material Genome Big-science Facilities Platform supported by Municipal Development and Reform Commission of Shenzhen.

Author contributions

Z.G. and L.H. conceived the study. Z.G. performed the first-principles calculations and theoretical analysis. H.Z., Z.W., and M.-U.F. conducted the phonon dispersion calculations and Monte Carlo simulations. L.B. commented on the paper. Z.G. and L.H. verified overall results and wrote the manuscript with input from all authors. All authors contributed to the discussion and interpretation of the data.

Competing interests

The authors declare no competing interests.

Additional information

Supplementary information The online version contains supplementary material available at https://doi.org/10.1038/s41524-024-01237-2.

Correspondence and requests for materials should be addressed to Li Huang.